THE ASTROPHYSICAL JOURNAL, 560:28–40, 2001 October 10

WINDOW FUNCTION FOR NONCIRCULAR BEAM COSMIC MICROWAVE BACKGROUND ANISOTROPY EXPERIMENT

TARUN SOURADEEP[1,2] AND BHARAT RATRA[1]

Received 2001 May 11; accepted 2001 June 5

ABSTRACT

We develop computationally rapid methods to compute the window function for a cosmic microwave background anisotropy experiment with a noncircular beam that scans over large angles on the sky. To concretely illustrate these methods we compute the window function for the Python V experiment, which scans over large angles on the sky with an elliptical Gaussian beam.

Subject headings: cosmic microwave background — cosmology: theory — methods: analytical — methods: data analysis

1. INTRODUCTION

Cosmic microwave background (CMB) anisotropy measurements are becoming an increasingly powerful tool for testing cosmogonies and constraining cosmological parameters. See, e.g., Subrahmanyan et al. (2000), Romeo et al. (2001), Dawson et al. (2001), and Padin et al. (2001) for recent CMB anisotropy observations and Ratra et al. (1997), Górski et al. (1998), Rocha et al. (1999), Gawiser & Silk (2000), Knox & Page (2000), Douspis et al. (2001), and Podariu et al. (2001) for discussions of constraints on models from the CMB anisotropy data.

Conventionally, the CMB temperature, $T(\gamma)$, is expressed as a function of angular position, $\gamma \equiv (\theta, \phi)$, on the sky via the spherical harmonic decomposition,

$$T(\gamma) = \sum_{\ell=0}^{\infty} \sum_{m=-l}^{l} a_{lm} Y_{lm}(\gamma) . \tag{1}$$

The CMB spatial anisotropy in a Gaussian model[3] is completely specified by its angular two-point correlation function $C(\gamma, \gamma') = \langle T(\gamma)T(\gamma')\rangle$, between directions γ and γ' on the sky. In most theoretical models the predicted fluctuations are statistically isotropic, $C(\gamma, \gamma') \equiv C(\gamma \cdot \gamma')$. The fluctuations can then be characterized solely by the angular spectrum C_l, defined in terms of the ensemble average,

$$\langle a_{lm} a_{l'm'}{}^* \rangle = C_l \, \delta_{ll'} \, \delta_{mm'} , \tag{2}$$

and related to the correlation function through

$$\langle T(\gamma)T(\gamma')\rangle = \sum_{l=0}^{\infty} [(2l + 1)/4\pi] C_l \, P_l(\gamma \cdot \gamma') , \tag{3}$$

where P_l is a Legendre polynomial.

Typically, a CMB anisotropy experiment probes a range of angular scales characterized by a window function $W_l(\gamma, \gamma')$.[4] To utilize the full information in the data one must use model anisotropy spectra (C_ls) defined over this range of angular scales. Such theoretical spectra are parameterized by cosmological parameters such as Ω_0, h, and Ω_B in these models[5] and by the spectrum of quantum fluctuations generated during inflation.

To use model C_ls in conjunction with CMB anisotropy data to estimate cosmological parameters, one must be able to carefully model the CMB anisotropy experiment, i.e., accurately compute the window function W_l. Given such a model of an experiment and a family of C_ls, one may optimize the fit to the data from the experiment either by using an (approximate) χ^2 technique (see, e.g., Ganga, Ratra, & Sugiyama 1996; Bond, Jaffe, & Knox 2000; Knox 1999; Rocha 1999; Lineweaver 2001; Dodelson 2000; Tegmark & Zaldarriaga 2000) or by using an exact maximum likelihood technique (see, e.g., Górski et al. 1995; Ganga et al. 1997, 1998; Ratra et al. 1998, 1999).

Current CMB anisotropy data are of significantly higher quality than data available just a few years ago. As a consequence, an accurate model of an experimental W_l must now account for effects that were ignored in earlier experiments. In this paper we develop computationally rapid methods that account for the noncircularity of the beam in a CMB anisotropy experiment window function at large angular separations where the curvature of the sky cannot be ignored. This must be accounted for in an experiment like Python V (Coble et al. 1999), which has an elliptical beam and samples a large enough area of the sky to

[1] Department of Physics, Kansas State University, Manhattan, KS 66506.
[2] Current address: IUCAA, Post Bag 4, Ganeshkhind, Pune 411007, India.

[3] The simplest inflation models predict a Gaussian CMB anisotropy (see, e.g., Fischler, Ratra, & Susskind 1985) on all but the smallest angular scales. CMB anisotropy observations on quarter-degree and larger angular scales appear to be Gaussian (see, e.g., Mukherjee, Hobson, & Lasenby 2000; Aghanim, Forni, & Bouchet 2001; Phillips & Kogut 2001; Park et al. 2001; Wu et al. 2001b; also see Podariu et al. 2001).

[4] See http://www.phys.ksu.edu/~tarun/CMBwindows/wincomb/wincomb_tf.html for a discussion and tabulation of zero-lag window functions.

[5] Here Ω_0 is the nonrelativistic-mass density parameter, h is the Hubble parameter in units of 100 km s^{-1} Mpc^{-1}, and Ω_B is the baryonic-mass density parameter.

prejudice use of the flat-sky approximation. While we focus here on Python V as a concrete illustrative example, our techniques are easily generalized to more complex cases (e.g., arbitrary beam shape, beam rotation, and non-Gaussianity of the beam). Wu et al. (2001a) develop an alternate method to deal with an asymmetric beam and apply this to the MAXIMA-1 experiment.

In § 2 we describe the general formalism for computing the window function. In §§ 3–5 we develop specific, computationally rapid methods for computing the window function in three different cases. The flat-sky approximation window function computation is covered in § 3. In § 4 we develop a general method, based on Wigner rotation functions, for computing the window function on a sphere and describe how to numerically implement this scheme. In § 5 we specialize to the case of an experiment like Python V, where long scans are performed at constant elevation, and provide a computationally rapid method for evaluating the exact window function. Approximate window functions obtained with the flat-sky approximation and from retaining only the first few terms in a perturbation expansion (in noncircularity about a circular beam) of the Wigner rotation functions method (hereafter Wigner method) are compared with the exact window function in § 6. We conclude in § 7. In the Appendix, we describe our parameterization and normalization of an elliptical Gaussian beam and also record analytic expressions for its Fourier and spherical harmonic transforms.

2. WINDOW FUNCTION COMPUTATION FORMALISM

Owing to the finite angular resolution of a CMB anisotropy experiment, the temperature "measured" by the experiment at point γ_i on the sky is

$$\tilde{T}(\gamma_i) = \int d\Omega_\gamma \, B(\gamma_i, \gamma) T(\gamma) \ . \tag{4}$$

Here $B(\gamma_i, \gamma)$ is the beam function that characterizes the angular dependence of the sensitivity of the apparatus around the pointing direction γ_i.

CMB anisotropy experiments that use a differencing or modulation scheme measure the difference in temperature between different points on the sky. The measured CMB temperature anisotropy in any differencing scheme (labeled below by index n) can be expressed as a weighted linear combination,

$$\Delta^{(n)}(\gamma_i) = \int d\Omega_\gamma \, w_i^{(n)}(\gamma) \tilde{T}(\gamma) \ , \tag{5}$$

where $w_i^{(n)}(\gamma)$ are the weight functions. In our discussion of Python V below, n corresponds to the harmonic number of cosine modulation weight functions. Instead of weights $w_i^{(n)}(\gamma)$ that are continuous functions, for Python V the weights $w_{ij}^{(n)}$ are discrete and characterize the sensitivity at γ_{ij}, the jth point on the discretized chopper cycle around the pointing direction γ_i. In this case the integral in equation (5) is replaced by a summation, and we have

$$\Delta^{(n)}(\gamma_i) = \sum_{j=1}^{N_c} w_{ij}^{(n)} \, \tilde{T}(\gamma_{ij}) \ , \tag{6}$$

where N_c is the number of points in the discretized chopper cycle.

The complete window function for modulation pair (n, m), $W_l^{(n,\, m)}(\gamma_i, \gamma_j)$, accounts for the effects of both the beam function and the differencing or modulation scheme of the experiment and is defined through the theoretical model covariance matrix

$$C_{ij}^{(n,\, m)} = \langle \Delta^{(n)}(\gamma_i)[\Delta^{(m)}(\gamma_j)]^* \rangle = \sum_{l=0}^{\infty} [(2l+1)/4\pi] C_l \, W_l^{(n,\, m)}(\gamma_i, \gamma_j) \ . \tag{7}$$

It proves convenient to distinguish between the window function's dependence on the finite angular resolution of the experimental apparatus (the beam function) and its dependence on the differencing scheme adopted for the experiment. Using equation (6), the complete theoretical covariance matrix element $C_{ij}^{(n,\, m)}$ between pixels i and j on the sky can be expressed as a weighted linear sum of single-beam correlation functions via

$$C_{ij}^{(n,\, m)} \equiv \sum_{p=1}^{N_c} \sum_{q=1}^{N_c} w_{ip}^{(n)} w_{jq}^{(m)} \langle \tilde{T}(\gamma_{ip}) \tilde{T}(\gamma_{jq}) \rangle \ . \tag{8}$$

We call the single-beam correlation function, $C^{(e)}(\gamma, \gamma') = \langle \tilde{T}(\gamma) \tilde{T}(\gamma') \rangle$, an elementary correlation function. The elementary correlation function does not depend on the differencing scheme used in the experiment but does depend on the beam function. We use $C^{(e)}$ to define what we call the (single-beam) elementary window function $W_l^{(e)}$ via

$$C^{(e)}(\gamma_i, \gamma_j) = \sum_{l=0}^{\infty} [(2l+1)/4\pi] C_l \, W_l^{(e)}(\gamma_i, \gamma_j) \ . \tag{9}$$

$W_l^{(e)}$ depends on the beam function of the experiment but not on the differencing strategy used. Using equations (8) and (9) the complete window function may be expressed as a weighted linear sum of elementary window functions via

$$W_l^{(n,\, m)}(\gamma_i, \gamma_j) = \sum_{p=1}^{N_c} \sum_{q=1}^{N_c} w_{ip}^{(n)} w_{jq}^{(m)} \, W_l^{(e)}(\gamma_{ip}, \gamma_{jq}) \ . \tag{10}$$

Using equations (3), (4), and (9), the elementary window function may be expressed as

$$W_l^{(e)}(\gamma_i, \gamma_j) = \int d\Omega_\gamma \, d\Omega_{\gamma'} \, B(\gamma_i, \gamma) B(\gamma_j, \gamma') P_l(\gamma \cdot \gamma') = [4\pi/(2l+1)] \sum_{m=-l}^{l} b_{lm}(\gamma_i)[b_{lm}(\gamma_j)]^* , \tag{11}$$

where

$$b_{lm}(\gamma_i) = \int d\Omega_\gamma \, B(\gamma_i, \gamma) Y_{lm}^*(\gamma) \tag{12}$$

is the spherical harmonic transform of the beam function pointing at γ_i.

For some experiments the beam function is accurately circularly symmetric about the pointing direction, i.e., $B(\gamma_i, \gamma) \equiv B(\gamma_i \cdot \gamma)$. This allows a great simplification,[6] because the beam function can then be represented as $B(\gamma_i \cdot \gamma) = (4\pi)^{-1} \sum_{l=0}^{\infty} (2l+1) B_l P_l(\gamma_i \cdot \gamma)$. Consequently, for a circularly symmetric beam function it is straightforward to derive the usual expression,

$$W_l^{(e)}(\gamma_i, \gamma_j) = B_l^2 \, P_l(\gamma_i \cdot \gamma_j) . \tag{13}$$

In addition to the single evaluation of the Legendre transform of the beam, B_l, computation of the elementary window function for an experiment with a circular beam simply involves computing P_l for all $l \leq l_{\max}$ using the stable upward recursion relation for each distinct pixel-pair separation. This is computationally inexpensive (at least by a factor $\sim l_{\max}$) compared with the computation of the elementary window function for an experiment with arbitrary beam shape (eq. [11]).

In the next three sections we discuss three cases in which one may compute the window function for an experiment with a noncircular beam in a time comparable to or just a factor of a few larger than that for the same experiment assuming a circular beam. First, we consider the flat-sky approximation, which is accurate if the experiment has a compact beam and the pixels are not separated by large angles (more precisely, the separation must be significantly less than a radian). This has been used previously for a number of experiments, including Python V (Coble et al. 1999; Coble 1999), MSAM (Coble 1999), and MAXIMA-1 (Wu et al. 2001a). Next, we develop a very general Wigner method that fully accounts for the curvature of the sky and accounts for the noncircularity of the beam in a perturbative expansion about a circular beam. In an experiment like Python V, where the noncircularity of the beam is not large, the first few terms in the noncircularity perturbation expansion provide sufficient accuracy. In this case the Wigner method allows one to compute the window function in a time a factor of a few larger than that for the corresponding circular-beam case. Finally, for an experiment that scans at constant elevation (such as Python V) with pixels lying on a small number of elevations, it is possible to implement a slightly different Wigner method that allows rapid computation of the exact window function for an arbitrary beam shape.

3. WINDOW FUNCTION IN THE FLAT-SKY APPROXIMATION

If an experiment scans a small enough patch of the sky, it is computationally advantageous to work in the flat tangent plane (rather than on the sphere) and make use of Fourier transforms (rather than spherical harmonic transforms) when modeling the experiment. See, e.g., Bond & Efstathiou (1987) and Coble (1999) for discussions. We may then transform from γ to coordinates in a locally flat patch, $\boldsymbol{\omega}$, and use a two-dimensional Fourier transform approximation to the spherical harmonic transform. For instance,

$$T(\boldsymbol{\omega}) = \int [d^2k/(2\pi)^2] \exp(i\boldsymbol{k} \cdot \boldsymbol{\omega}) T(\boldsymbol{k}) . \tag{14}$$

Here $\boldsymbol{\omega} = (\omega, \phi)$, are polar coordinates in the neighborhood of the north pole γ_{P} in the patch on the sky, i.e., $\gamma = \gamma_{\mathrm{P}} + \boldsymbol{\omega}$, or $\boldsymbol{\omega} = (\omega_1, \omega_2) = (\omega \cos\phi, \omega \sin\phi)$, where $\omega = 2\sin(\theta/2) = |\gamma - \gamma_p|$, $0 \leq \omega \leq 2$, and θ is the colatitude (see, e.g., Bond & Efstathiou 1987). In the small-angle approximation, the ensemble average of the Fourier transform of the temperature is

$$\langle T(\boldsymbol{k}) T^*(\boldsymbol{k}') \rangle = (2\pi)^2 C_k \, \delta^{(2)}(\boldsymbol{k} - \boldsymbol{k}') , \tag{15}$$

where $k = |\boldsymbol{k}|$ and C_k is the CMB anisotropy power spectrum. This flat-sky analog of equation (2) is obtained assuming statistical homogeneity on the flat sky. The angular correlation function can then be expressed as

$$\langle T(\boldsymbol{\omega}_i) T(\boldsymbol{\omega}_j) \rangle = (1/2\pi) \int_0^\infty dk \, k J_0(k|\boldsymbol{\omega}_i - \boldsymbol{\omega}_j|) C_k , \tag{16}$$

where J_0 is the zeroth-order Bessel function of the first kind. Comparing this expression with equation (3) in the small angular separation and large-l regime where $P_l(\cos\theta) \rightarrow J_0([l + 1/2]\theta)$, we arrive at the correspondence $k \sim l + 1/2$ between the radial wavenumber on the flat sky k and the spherical multipole l.

For an experiment for which the flat-sky approximation is valid, the "measured" temperature (see eq. [4]) is

$$\tilde{T}(\boldsymbol{\omega}_i) = \int [d^2k/(2\pi)^2] \exp(i\boldsymbol{k} \cdot \boldsymbol{\omega}_i) B(\boldsymbol{R}_i[\boldsymbol{k}]) T(\boldsymbol{k}) , \tag{17}$$

[6] When the beam is pointing toward a pole, γ_{P}, the coefficients in the spherical harmonic expansion of a circular beam function are $b_{lm}(\gamma_{\mathrm{P}}) = B_l[(2l+1)/4\pi]^{1/2}\delta_{m0}$. Here δ_{m0} is a Kronecker delta function and implies that the only nonzero spherical harmonic coefficients are those that result in a circularly symmetric beam function.

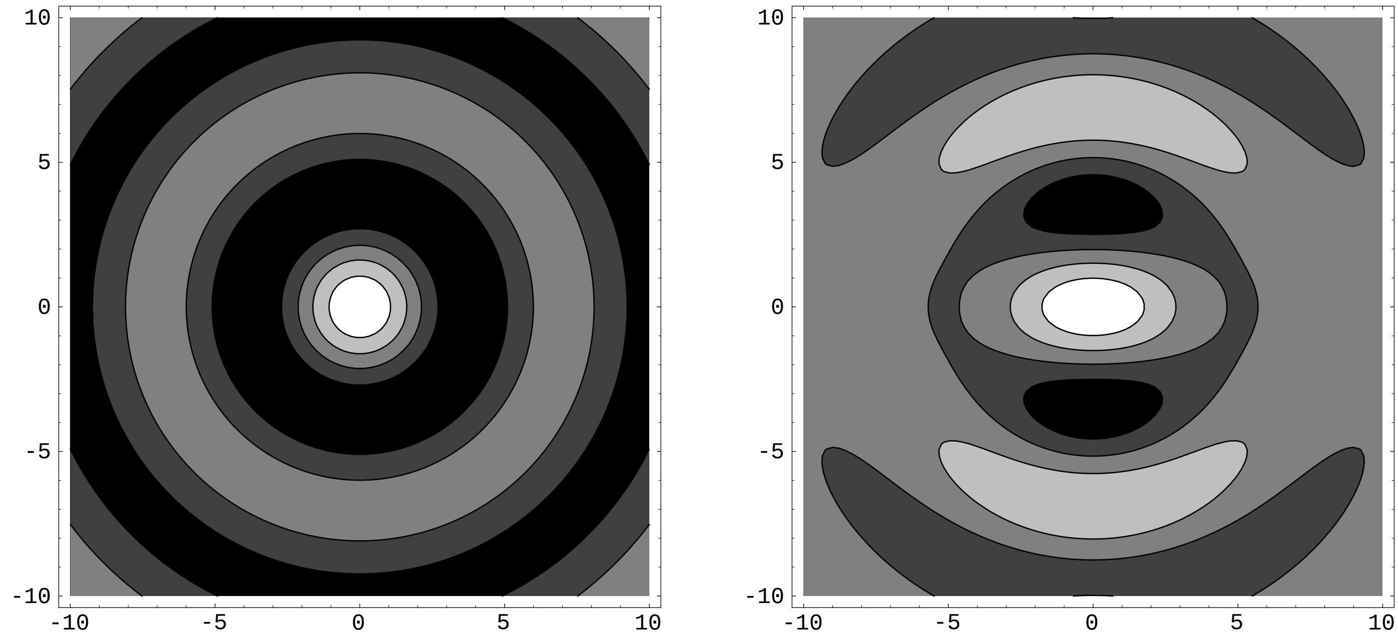

FIG. 1.—Contour plots of the zeroth-order (eq. [22]; *left*) and first-order (eq. [23]; *right*) terms in the noncircularity perturbation expansion of the flat-sky approximation elementary window function for an elliptical Gaussian beam function experiment. These are computed for the nominal FWHM beamwidths of the Python V experiment, 1°.02 in elevation and 0°.91 in azimuth. They are plotted as a function of dimensionless variables $k\boldsymbol{x}$, and the two panels are centered on the center of the zeroth-order, circular-beam window function. As expected, the flat-sky window function for the circular beam in the left panel is circularly symmetric. For a fixed value of k, the first-order correction in the right panel must be multiplied by $-k^2(\sigma_2^2 - \sigma_1^2)$ before being added to the zeroth-order term. For Python V the higher order terms are small compared to the first-order term and visually have roughly similar structure.

where $B(\boldsymbol{k})$ is the Fourier transform of the beam function pointing at the origin $\boldsymbol{\omega} = 0$ of the local flat coordinate patch. The rotation operator $\boldsymbol{R}_i$ (which rotates $\boldsymbol{k}$ by an angle ϱ_i) accounts for a possible rotation of the telescope beam pointing at $\boldsymbol{\omega}_i$ relative to the telescope beam pointing at the origin. In addition to the case in which the telescope physically rotates around its axis as it moves from one pointing direction to another, nonzero values of ϱ_i can arise when the telescope is not located at a Pole and also when a single flat-sky coordinate system is set up on a patch large enough for sky curvature to be important. In the latter two cases, this rotation is important only in the regime where one expects the flat-sky approximation to be poor.

The modulated temperature $\Delta^{(n)}(\gamma_i)$, expressed in terms of $\tilde{T}(\boldsymbol{\omega}_{ij})$, is given by equation (6). The window function $W_l^{(n,\,m)}(\gamma_i, \gamma_j)$ is defined through the covariance matrix by

$$C_{ij}^{(n,\,m)} = \sum_{l=0}^{\infty} \frac{(2l+1)}{4\pi} C_l W_l^{(n,m)}(\gamma_i, \gamma_j) \simeq \int_0^{\infty} \frac{dk}{2\pi} k C_k W_k^{(n,m)}(\gamma_i, \gamma_j) , \tag{18}$$

where we identify the flat space radial wavenumber k with $l + 1/2$. The complete window function $W_k^{(n,\,m)}(\gamma_i, \gamma_j)$ may be expressed in terms of elementary window functions $W_k^{(e)}$ by using equation (10).

Using equations (9) and (17), the expression for the elementary window function in the flat-sky approximation is

$$W_k^{(e)}(\boldsymbol{\omega}_i, \boldsymbol{\omega}_j) = \int_0^{2\pi} \frac{d\phi_k}{2\pi} \exp\,[i\boldsymbol{k} \cdot (\boldsymbol{\omega}_i - \boldsymbol{\omega}_j)] B(\boldsymbol{R}_i[\boldsymbol{k}]) B^*(\boldsymbol{R}_j[\boldsymbol{k}]) . \tag{19}$$

Further analytical manipulations are needed to derive an expression suitable for numerical evaluation. Without loss of generality, we transform to a new, flat-coordinate system with $\boldsymbol{\omega}_i$ as the origin: $\boldsymbol{\omega}'_i = (0, 0)$ and $\boldsymbol{\omega}'_j = (\omega'_1, \omega'_2)$. In what follows we drop the prime on the new coordinates. For small angular separations, $\omega = |\boldsymbol{\omega}_i - \boldsymbol{\omega}_j| \ll 1$ (and ignoring rotations, $\varrho_j = 0$), we have

$$W_k^{(e)}(\boldsymbol{\omega}_i, \boldsymbol{\omega}_j) = \int_0^{2\pi} (d\phi_k/2\pi) \;\; \cos\,[k\omega \cos\,(\phi_k - \alpha)] B(\boldsymbol{k}) B^*(\boldsymbol{k}) , \tag{20}$$

where we have defined $\alpha = \tan^{-1}(\omega_2/\omega_1)$.

For an elliptical Gaussian beam function (eq. [A1]), an analytic expression for $B(\boldsymbol{k})$ is given in equation (A7). Using this in equation (20), we obtain

$$W_k^{(e)}(\boldsymbol{\omega}_i, \boldsymbol{\omega}_j) = \int_0^{\pi} (d\phi_k/\pi) \cos\,[k\omega \cos\,(\phi_k - \alpha)] \exp\,[-k^2 {\sigma_1}^2 (1 + \varepsilon \sin^2 \phi_k)] , \tag{21}$$

where σ_1 and σ_2 are the beamwidths (in radians) along the major and minor axis of the elliptical Gaussian beam. It is useful to define the rms beamwidth $\sigma_{\rm rms}$ as $[({\sigma_1}^2 + {\sigma_2}^2)/2]^{1/2}$, and a measure of the noncircularity of the elliptical beam ε as $(\sigma_2/\sigma_1)^2 - 1$.

The expression for the flat-sky window function for an elliptical Gaussian beam given in equation (21) can be readily evaluated numerically. It can also be expressed analytically as an infinite series expansion, $W_k^{(e)} = \sum_{n=0}^{\infty}(-1)^n b_k^n\, {}^{(n)}W_k^{(e)}$, in powers of an anisotropy or noncircularity parameter, $b_k = \varepsilon(\sigma_1 k)^2 = k^2({\sigma^2}_2 - {\sigma^2}_1)$. The series is perturbative ($b_k < 1$) up to multipoles $l \lesssim |\sigma_2^2 - \sigma_1^2|^{-1/2}$, which can be considerably larger than the inverse of the rms beamwidth $\sigma_{\rm rms}$. As expected, the first ($n = 0$) term in this series corresponds to the circular beam function result ($\sigma_1 = \sigma_2 = \sigma$),

$$ {}^{(0)}W_k^{(e)}(\omega_i, \omega_j) = J_0(k\omega) \exp(-k^2 {\sigma_1}^2) . \tag{22} $$

For a noncircular Gaussian beam function the next two terms are

$$ {}^{(1)}W_k^{(e)}(\omega_i, \omega_j) = \left[\frac{J_1(k\omega)}{k\omega} - J_2(k\omega) \sin^2 \alpha\right] \exp(-k^2 {\sigma_1}^2) \tag{23} $$

and

$$ {}^{(2)}W_k^{(e)}(\omega_i, \omega_j) = (1/2)\left[3\,\frac{J_2(k\omega)}{(k\omega)^2} - 6\,\frac{J_3(k\omega)}{k\omega} \sin^2 \alpha + J_4(k\omega) \sin^4 \alpha\right] \exp(-k^2 {\sigma_1}^2) , \tag{24} $$

where $J_m(x)$ is the mth-order Bessel function of the first kind. At arbitrary order n the term is

$$ {}^{(n)}W_k^{(e)}(\omega_i, \omega_j) = \frac{\sqrt{\pi}\,\Gamma(n + 1/2)}{\Gamma(n + 1)} \exp(-k^2 {\sigma_1}^2) \sum_{m=0}^{n} \frac{(\sin \alpha)^{2m}(\cos \alpha)^{2(n-m)}}{\Gamma(n - m + 1)\Gamma(m + 1)}\, {}_1F_2\left[\frac{1}{2} + m, \left(\frac{1}{2}, 1 + n\right), -\frac{(k\omega)^2}{4}\right] , \tag{25} $$

where Γ is the Euler gamma function and ${}_1F_2$ is a generalized hypergeometric function. Figure 1 shows contour plots of the zeroth-order (eq. [22]) and first-order (eq. [23]) terms in the noncircularity expansion of the flat-sky window function. These are computed for parameter values characterizing the Python V experiment (see § 6 below for details of the experiment).

4. WIGNER-METHOD WINDOW FUNCTION

If an experiment takes data over a large enough area of the sky, the formalism developed in the previous section, based on the flat-sky approximation, cannot be used to compute the window function. In this section we develop a general method for computing the window function for an experiment with an arbitrary beam shape that collects data from a large area on the sky.

For pointing direction $\gamma_i = (\theta_i, \phi_i)$ and vector in the beam $\gamma = (\theta, \phi)$, the beam function may be expanded in a spherical harmonic decomposition,

$$ B(\gamma_i, \gamma) = \sum_{l=0}^{\infty} \sum_{m=-l}^{l} b_{lm}(\gamma_i) Y_{lm}(\gamma) . \tag{26} $$

Here the expansion coefficients, $b_{l\,m}$, are given by equation (12).

For ease of computation it is convenient to rotate to a new coordinate system in which the new $\boldsymbol{x}_3'$-axis lies along the pointing direction γ_i. This is accomplished by first rotating the coordinate system around the $\boldsymbol{x}_3$-axis by ϕ_i and then rotating around the new $\boldsymbol{x}_2'$- axis by θ_i. Then

$$ B(\boldsymbol{x}_3', \gamma') = \sum_{l'=0}^{\infty} \sum_{m'=-l'}^{l'} b_{l'm'}(\boldsymbol{x}_3') Y_{l'm'}(\gamma') = B(\gamma_i, \gamma) , \tag{27} $$

where the last step follows from the fact that B is a scalar.

If the experiment is not located at a Pole, the beam of a telescope that does not rotate around its beam axis will, nevertheless, seem to "rotate" around the beam axis with respect to the local azimuth and declination directions. Hence, we allow for a rotation ϱ_i of the beam around the beam axis relative to a parallel transport of the beam on the sky from the Pole $\gamma_{\rm P}' = \boldsymbol{x}_3'$ to the pointing direction γ_i'. The Python V experiment was located at the South Pole and hence has $\varrho_i = 0$. The rotation ϱ_i can also account for noncircular beam function cases where the telescope rotates around its axis as it moves from one pointing direction to another (e.g., one mounted on a satellite).

The rotations discussed in the previous two paragraphs correspond to Euler angles $\alpha = \phi_i$, $\beta = \theta_i$, and $\gamma = \varrho_i$ in the notation of scheme A of § 1.4.1 of Varshalovich, Moskalev, & Khersonskii (1988, hereafter VMK). From equation (1) of their § 5.5.1 we have

$$ Y_{l'm'}(\gamma') = \sum_{m''=-l'}^{l'} Y_{l'm''}(\gamma) D^{l'}{}_{m''m'}(\phi_i, \theta_i, \varrho_i) , \tag{28} $$

where $D^{l'}{}_{m''m'}$ is a Wigner D-function corresponding to the rotation of the beam. From equations (28) and (27) we have

$$ b_{lm}(\gamma_i) = \sum_{m'=-l}^{l} b_{lm'}(\mathbf{x}_3') D^l_{mm'}(\phi_i, \theta_i, \varrho_i) . \tag{29} $$

We focus on the elementary window function, i.e., ignore the modulation and consider the window function for two points γ_i and γ_j (see eq. [11]). Using the usual decomposition for the Legendre polynomial in terms of spherical harmonics, the fact that B is real, and equations (28) and (29), we find

$$ W_l^{(e)}(\gamma_i, \gamma_j) = [4\pi/(2l + 1)] \sum_{m'=-l}^{l} \sum_{m''=-l}^{l} [b_{lm'}(\boldsymbol{x}_3')]^* b_{lm''}(\boldsymbol{x}_3') \sum_{m=-l}^{l} [D^l_{mm'}(\phi_i, \theta_i, \varrho_i)]^* D^l_{mm''}(\phi_j, \theta_j, \varrho_j) . \tag{30} $$

When the beam function is circularly symmetric $b_{lm}(\boldsymbol{x}'_3) = \delta_{m0} B_l[(2l+1)/4\pi]^{1/2}$. Using $D^l_{m0}(\theta, \phi, \varrho) = [4\pi/(2l+1)]^{1/2} Y_{lm}(\theta, \phi)$, it is straightforward to establish that in this case equation (30) reduces to the usual expression given in equation (13).

Using the addition theorem for Wigner D-functions (eqs. [2] of § 4.4, [1] of § 4.3, and [5] and [6] of § 4.7.2 of VMK), we reduce equation (30) to the simpler form,

$$W_l^{(e)}(\gamma_i, \gamma_j) = [4\pi/(2l+1)] \sum_{m'=-l}^{l} \sum_{m''=-l}^{l} [b_{lm'}(\boldsymbol{x}'_3)]^* b_{lm''}(\boldsymbol{x}'_3) D^l_{m'm''}(\alpha - \varrho_i, \gamma, \beta + \varrho_j) , \tag{31}$$

where

$$\begin{aligned} \cos\gamma &= \cos\theta_i \cos\theta_j + \sin\theta_i \sin\theta_j \cos(\phi_i - \phi_j) = \gamma_i \cdot \gamma_j , \\ \cot\alpha &= -\cos\theta_i \cot(\phi_i - \phi_j) + \sin\theta_i \cot\theta_j \csc(\phi_i - \phi_j), \\ \cot\beta &= -\cos\theta_j \cot(\phi_i - \phi_j) + \cot\theta_i \sin\theta_j \csc(\phi_i - \phi_j) . \end{aligned} \tag{32}$$

For large values of l it is computationally expensive to evaluate the entire m' and m'' sum in equation (31). However, for a smooth, mildly noncircular beam function (defined precisely below), restricting the summation to a few low values of m' and m'' results in a good approximation. A smooth (i.e., not sharply peaked) beam function results in b_{l0} falling off with increasing l. At large l and small γ, $D^l_{mm'}(\alpha, \gamma, \beta) \to \exp(-im\alpha - im'\beta) J_{|m-m'|}([l+1/2]\gamma)$. Thus, the $D^l_{m'm''}$ term in equation (31) strongly suppresses, as $(l\gamma)^{|m'-m''|}$, the contribution from off-diagonal $m' \neq m''$ terms. In addition, mild noncircularity requires that at each value of l the ratio $|b_{lm}/b_{l0}|$ decrease rapidly with increasing $|m|$. Hence, the products $b^*_{lm'} b_{lm''}$, as functions of l, are ordered in magnitude and falloff as one goes to higher values of $|m'| + |m''|$. For Python V, in which the deviation from circularity is small, retaining the first nonzero-order term is sufficient for computing an accurate covariance function.[7]

We now derive explicit expressions for the first few leading-order terms in equation (31) for the specific case of an elliptical beam function. For an elliptical-beam function, symmetry dictates that $b_{lm}(\boldsymbol{x}'_3) = 0$ for odd m (see the Appendix). In what follows, beam rotations are set to zero ($\varrho_i = 0$), but it is straightforward to restore them from the complete expression given above. The zeroth-order term contains D^l_{00}, the first-order term has four contributors (D^l_{02}, $D^l_{0,-2}$, D^l_{20}, and $D^l_{-2,0}$), and the second-order term has eight contributors (D^l_{22}, $D^l_{2,-2}$, $D^l_{-2,2}$, $D^l_{-2,-2}$, D^l_{04}, $D^l_{0,-4}$, D^l_{40}, and $D^l_{-4,0}$).

After a significant amount of algebraic manipulation (using equations from §§ 4.3, 4.4, 4.8, and 4.17 of VMK, familiar properties of Legendre polynomials and modified Bessel functions, and the reality condition on the beam, eq. [A8]), we find a series expansion of the elementary window function,

$$\begin{aligned} W_l^{(e)}(\gamma_i, \gamma_j) = \frac{4\pi}{2l+1} \{ & [b_{l0}(\boldsymbol{x}'_3)]^2 d^l_{00}(\gamma) + 2b_{l0}(\boldsymbol{x}'_3) b_{l2}(\boldsymbol{x}'_3)[\cos(2\alpha) + \cos(2\beta)] d^l_{02}(\gamma) \\ & + 2[b_{l2}(\boldsymbol{x}'_3)]^2 [\cos(2\alpha + 2\beta) d^l_{22}(\gamma) + (-1)^{-l} \cos(2\alpha - 2\beta) d^l_{22}(\pi - \gamma)] \\ & + 2b_{l0}(\boldsymbol{x}'_3) b_{l4}(\boldsymbol{x}'_3)[\cos(4\alpha) + \cos(4\beta)] d^l_{04}(\gamma) + \cdots \} . \end{aligned} \tag{33}$$

Here the angles α, β, and γ are defined in equation (32), and the $d^l_{mm'}$s are the usual Wigner d-functions of angular momentum theory (see, e.g., § 4.3 of VMK) related to the Wigner D-functions through $D^l_{mm'}(\alpha, \gamma, \beta) = e^{-im\alpha} d^l_{mm'}(\gamma) e^{-im'\beta}$. More precisely,

$$\begin{aligned} d^l_{00}(\gamma) &= P_l(\cos\gamma) , \\ d^l_{02}(\gamma) &= -[l(l+1)/(l-1)(l+2)]^{1/2} P_l(\cos\gamma) + \{2\cos\gamma/[(l-1)l(l+1)(l+2)]^{1/2}\} P'_l(\cos\gamma) , \\ d^l_{22}(\gamma) &= \frac{1}{(l-1)(l+2)} \left[-4\left(\frac{2-\cos\gamma}{1+\cos\gamma}\right) + l(l+1) \right] P_l(\cos\gamma) + \frac{4(1-\cos\gamma)}{(l-1)l(l+1)(l+2)} \left[-\left(\frac{2-\cos\gamma}{1+\cos\gamma}\right) + l(l+1) \right] P'_l(\cos\gamma) , \\ d^l_{22}(\pi-\gamma) &= \frac{(-1)^l}{(l-1)(l+2)} \left[-4\left(\frac{2+\cos\gamma}{1-\cos\gamma}\right) + l(l+1) \right] P_l(\cos\gamma) \\ &\quad + \frac{4(-1)^{l+1}(1+\cos\gamma)}{(l-1)l(l+1)(l+2)} \left[-\left(\frac{2+\cos\gamma}{1-\cos\gamma}\right) + l(l+1) \right] P'_l(\cos\gamma) , \\ d^l_{04}(\gamma) &= -l(l+1)[(l-4)!/(l+4)!]^{1/2} \left[\frac{6(1+3\cos^2\gamma)}{\sin^2\gamma} - l(l+1) \right] P_l(\cos\gamma) \\ &\quad + 8[(l-4)!/(l+4)!]^{1/2} \cos\gamma \left[\frac{3(1+\cos^2\gamma)}{\sin^2\gamma} - l(l+1) \right] P'_l(\cos\gamma) , \end{aligned} \tag{34}$$

where $P'_l \equiv dP_l(x)/dx$. Recursion relations in the indices l, m, and m' (see VMK) can be used to compute $d^l_{mm'}$ for larger values of m and m'.

Evaluating the first few terms of the Wigner-method expansion in equation (33) involves computing P_l and P'_l. The first derivative, P'_l, can be readily computed in terms of P_l and P_{l-1} during the generation of P_l, using the upward recursion

[7] By a sufficiently accurate covariance function we mean that the maximum likelihood analysis results are not significantly affected by higher order corrections. This criterion of sufficient accuracy therefore depends on the level of noise in the experiment, which is encoded in the noise covariance matrix of the experiment.

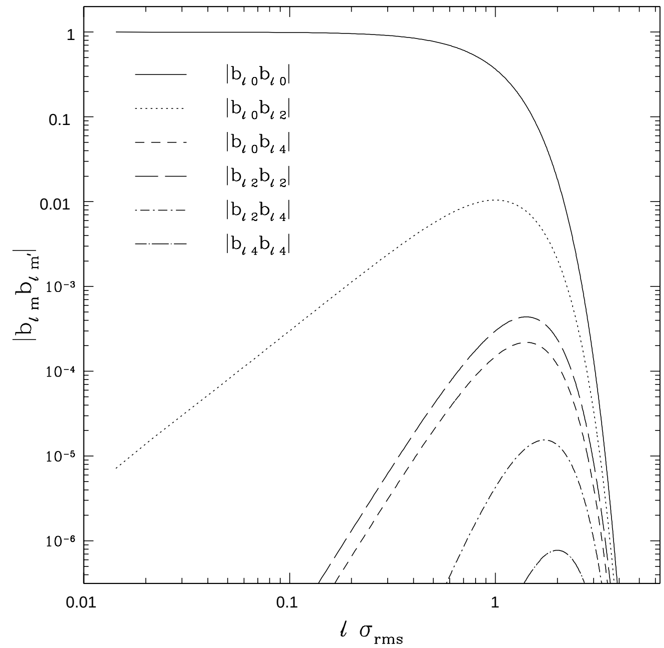

FIG. 2.—Coefficients $|b_{lm}(x'_3)b_{lm'}(x'_3)|$ of the six lowest-order terms in the perturbation expansion of the Wigner-method elementary window function (see eqs. [33] and [31]). These are computed for the elliptical Gaussian Python V beam function and plotted as a function of $l\sigma_{rms}$. For the Python V beam function the ellipticity parameter $\epsilon = 0.26$. Noncircularity corrections are important for $l\sigma_{rms} > 1$. Note that the peak shifts to higher values of l for higher order terms, relative to the peak position for lower order coefficients. The shapes of the curves are independent of σ_{rms} but depend sensitively on the beam-function ellipticity.

relation. Hence, the computational cost of evaluating $W_l^{(e)}$ for a mildly noncircular beam function (using eq. [33]) is only a factor of a few larger than that for a circular beam function.

Figure 2 shows, as a function of $l\sigma_{rms}$, the six leading-order $|b_{lm}(x'_3)b_{lm'}(x'_3)|$ coefficients (with m, $m' = 0$, 2, and 4) of the expansion of equation (31) (see eq. [33]) for the Python V experiment. These are also the leading-order contributors to the zero-lag elementary window function. Note that the curves do not cross at any l, i.e., the ordering of the coefficients is maintained for all l, and at large l (past the peak) higher order terms fall off more rapidly with l. Hence this perturbation expansion is an efficient scheme for computing noncircularity corrections. The noncircularity corrections peak at angular scales smaller than the rms beamwidth σ_{rms}. Thus, noncircularity corrections are not that important for an elementary

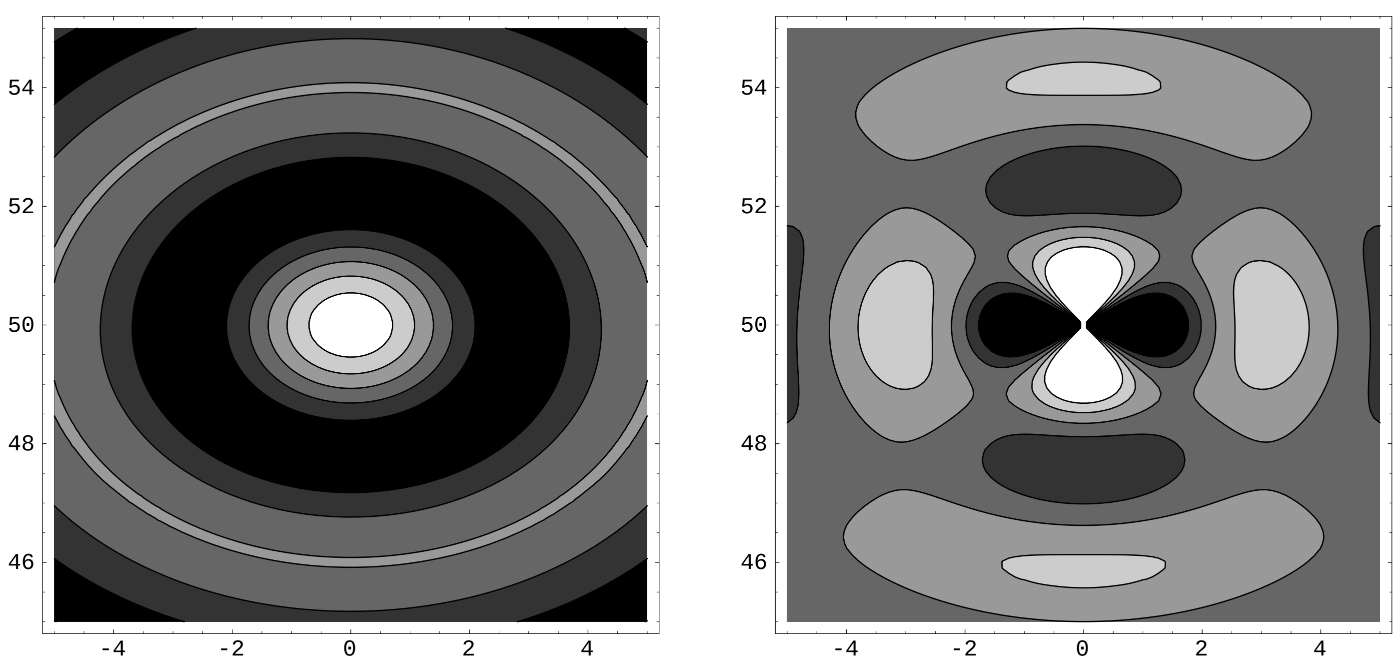

FIG. 3.—Contour plots in the azimuth-declination plane (with azimuth along the horizontal axis) of terms in the Wigner-method perturbation expansion of the elementary window function for the Python V experiment. These are plotted for multipole $l = 100$ such that $l\sigma_{rms} \sim 1$. The left panel shows the zeroth-order isotropic term $d^l_{00}(\gamma)$, and the right panel shows the first-order correction term $[\cos(2\alpha) + \cos(2\beta)]d^l_{02}(\gamma)$ (see eq. [33]). Here γ is the angular separation between the central pixel and the pixel at the given azimuthal and declination sky coordinates.

window function (a single-beam experiment), but they can have a significant effect on the complete window function for a modulated experiment if the modulation scheme results in sensitivity to the $l\sigma_{\rm rms} > 1$ regime.

Figure 3 shows contour plots of the isotropic term $d^l_{00}(\gamma)$ and the leading-order correction term $[\cos(2\alpha) + \cos(2\beta)]d^l_{02}(\gamma)$ in the perturbation expansion of the Wigner-method elementary window function (see eq. [33]) for the Python V experiment. These are plotted for multipole $l = 100$ chosen so that $l\sigma_{\rm rms} \sim 1$, which is where the noncircularity correction starts becoming significant. Close to the center of the plots this noncircularity correction is larger along the major and minor axes of the elliptical beam. The correction term falls off with increasing pixel separation, suggesting that the circular beam function approximation is good for sufficiently large separations. Also, for a modestly noncircular beam function this implies that higher order terms in the Wigner-method perturbation expansion need be retained only for close pixel pairs and hence that one can truncate the summation in equation (31) at lower orders for progressively more widely separated pixel pairs.

5. CONSTANT-ELEVATION SCAN WINDOW FUNCTION

For an experiment, such as Python V, that scans at constant elevation,[8] it is possible to derive another expression for the window function, one that does not require use of the approximation of the previous section (the truncation of the m' and m'' series).

We follow the initial development of the previous section and transform to a new coordinate system by rotating around the $\boldsymbol{x}_3$-axis by ϕ_i, where $\gamma_i = (\theta_i, \phi_i)$ is the pointing direction. The Euler angles of this rotation are $\alpha = \phi_i$, $\beta = 0$, and $\gamma = \varrho_i$. As described in the previous section, ϱ_i represents a relative rotation of the beam around its axis. For an experiment located at one of the Poles $\varrho_i = 0$. In general, we have

$$b_{lm}(\gamma_i) = \sum_{m'=-l}^{l} b_{lm'}(\boldsymbol{x}'_3) D^l_{mm'}(\phi_i, 0, \varrho_i) . \tag{35}$$

From § 4.16 of VMK we find $D^l_{mm'}(\phi_i, 0, \varrho_i) = \exp[-im(\phi_i + \varrho_i)]\delta_{mm'}$. Equation (35) then implies $b_{lm}(\theta_i, \phi_i) = \exp[-im(\phi_i + \varrho_i)]b_{lm}(\theta_i, 0)$ and so equation (30) reduces to

$$W^{(e)}_l(\gamma_i, \gamma_j) = [4\pi/(2l + 1)] \sum_{m=-l}^{l} \exp\{-im[(\phi_i - \phi_j) + (\varrho_i - \varrho_j)]\} b^*_{lm}(\theta_i, 0) b_{lm}(\theta_j, 0) . \tag{36}$$

Window functions between pixels lying on a few constant-elevation lines can be rapidly computed by using equation (36) and precomputed $b_{lm}(\theta_i, 0)$-values.

For an experiment, such as Python V, whose beam function has the symmetry $B(\theta_i, 0; \theta, \phi) = B(\theta_i, 0; \theta, -\phi)$, it may be shown that equations (12) and (26) and the fact that the beam function B is real imply that $b_{lm}(\theta_i, 0)$ is real. In this case equation (36) may be reexpressed as

$$W^{(e)}_l(\gamma_i, \gamma_j) = [4\pi/(2l + 1)] \sum_{m=-l}^{l} \cos\{m[(\phi_i - \phi_j) + (\varrho_i - \varrho_j)]\} b_{lm}(\theta_i, 0) b_{lm}(\theta_j, 0) . \tag{37}$$

Here $b_{lm}(\theta, 0)$ is defined in the usual way through equation (12). For the Python V experiment, which chops at constant elevation and in which the pixels lie on a relatively small number of elevations,[9] it is possible to precompute and store the $b_{lm}(\theta, 0)$-values at all elevations θ. Given these precomputed b_{lm}-values, the elementary window function can be computed very rapidly by using equation (37).

6. COMPARISON OF APPROXIMATE AND EXACT PYTHON V COVARIANCE MATRICES

Python V is a CMB anisotropy experiment that performs wide-angle scans with a noncircular beam. In this section, we compare Python V window functions with theoretical covariance matrices computed in the flat-sky approximation and in the Wigner-method perturbative approximation, as well as in the exact method.

Python V observations were made at 37–45 GHz. Two regions of the sky were observed: the main field, a rectangle 7°.5 in declination ($\delta = -52°$ to $-45°.4$) by 67°.7 in azimuth (centered on $\alpha = 23^{\rm h}.18$), and another rectangular patch 3° in declination ($\delta = -63°$ to $-60°$) by 30° in azimuth (centered on $\alpha = 3^{\rm h}.0$). For detailed descriptions of the experiment and data see Coble et al. (1999) and Coble (1999).

The Python V beam function is well described by an elliptical Gaussian with FWHM beamwidths of $1°.02^{+0°.03}_{-0°.01}$ in elevation and $0°.91^{+0°.03}_{-0°.01}$ in azimuth (one standard deviation uncertainties). The Python V beam function is a compact elliptical Gaussian (eq. [A1]) with $\sigma_1 = 0.0076$ and $\sigma_2 = 0.0067$ as the nominal beamwidths in radians. Python V uses a constant-elevation, smoothly scanning sampling strategy around every pixel on the sky, with a chopper throw (end to end) of $\Phi_c = 17°.06$. Each chopper cycle consists of 128 time samples suitably modulated in time to correspond to the spatial modulations described below. To compute the window function we need to know only the final spatial modulation strategy adopted. See Coble (1999) for a more detailed discussion of these procedures. The constant-elevation scans are discretely resampled in space (with ninefold oversampling) at $N_c = 567$ equispaced points (θ_i, ϕ^p_i) labeled by integers $p = 1, 2, \ldots, N_c$ along the chopper cycle around the pixel $\gamma_i = (\theta_i, \phi_i)$. The azimuth $\phi^p_i = \phi_i + (p - 1)\Delta\phi + (\Phi_o - \Phi_c/2)$, where $\Delta\phi = \Phi_c/(N_c - 1)$ is the spacing between points and $\Phi_o = 0°.58$ accounts for the offset between the azimuth of the pixel, ϕ_i, and the center of scan. The scans are modulated using the first eight cosine harmonics of the chopper cycle (hereafter modulations 1–8). All

[8] Constant elevation here refers most generally to any set of parallel circles on the sky.

[9] The 690 sky pixels of Python V lie on 11 distinct elevations.

modulations, other than the first, are apodized by a Hann window to reduce ringing in multipole space and down weight data taken during chopper turnaround. For the modulated Python V scans the weight functions (see eq. [6]) are[10]

$$w_{ip}^{(m)} = 2M_p^{(m)} \Big/ \sum_{p=1}^{N_c} |M_p^{(m)}| \,, \tag{38}$$

where

$$\begin{aligned} M_p^{(1)} &= \cos(2\pi Z_p) \\ M_p^{(m)} &= [(-1)^{m+1}/2]\cos(2\pi m Z_p)[1-\cos(2\pi Z_p)] \,, \qquad (m>1) \,, \end{aligned} \tag{39}$$

with $Z_p = (p-1)/(N_c-1)$. These weights are used to obtain the Python V complete window function $W_l^{(n,m)}(\gamma_i, \gamma_j)$ (between modulation m of the scan around sky pixel γ_i and modulation n of the scan around sky pixel γ_j) in terms of the elementary window functions (see eq. [10]).

The $M_p^{(m)}$ are identical for all pixels; hence, $w_{ip}^{(m)}$ is independent of pixel index i. With identical constant-elevation chops around every pixel, equation (10) can be reexpressed in a computationally more efficient form. In this case, the elementary window function $W_l^{(e)}$ depends only on $\phi_i^p - \phi_j^q$ (at fixed θ_i and θ_j). This reduces the number of separations at which $W_l^{(e)}$ is needed and thus speeds up the computation. In this case we may reexpress the window function as

$$\begin{aligned} W_l^{(n,m)}(\gamma_i, \gamma_j) = & \sum_{q_1=1}^{N_c-1} \sum_{q_2=1}^{N_c-q_1} \left[w_{i(q_2+q_1)}^{(n)} w_{jq_2}^{(m)} W_l^{(e)}(\theta_i, \theta_j, \phi_i - \phi_j + q_1 \Delta\phi) + w_{iq_2}^{(n)} w_{j(q_2+q_1)}^{(m)} W_l^{(e)}(\theta_i, \theta_j, \phi_i - \phi_j - q_1 \Delta\phi) \right] \\ & + \sum_{q_2=1}^{N_c-1} w_{iq_2}^{(n)} w_{jq_2}^{(m)} W_l^{(e)}(\theta_i, \theta_j, \phi_i - \phi_j) \,. \end{aligned} \tag{40}$$

Here the three arguments of the elementary window functions (the three $W_l^{(e)}$ between two directions) are the colatitudes of the two directions and the difference in their azimuth angles. Precomputing the second summations over the weight products, $\varpi_p^{(m,n)} = \sum_{q=1}^{N_c-p} w_{i(q+p)}^{(n)} w_{jq}^{(m)}$, for the set of all the modulation pairs speeds up the evaluation of the right-hand side of equation (40).

Figure 4 shows the eight equal-modulation, exact Python V zero-lag complete window functions at the two extreme values of the declination, $\delta = -63°$ and $\delta = -45°.4$. Also plotted for comparison is the zero-lag elementary window function at $\delta = -63°$. The effect of beam function noncircularity is more pronounced for the modulated (complete) window functions,

[10] The following expressions correct a typographical error in the corresponding expressions in Coble et al. (1999) and Coble (1999).

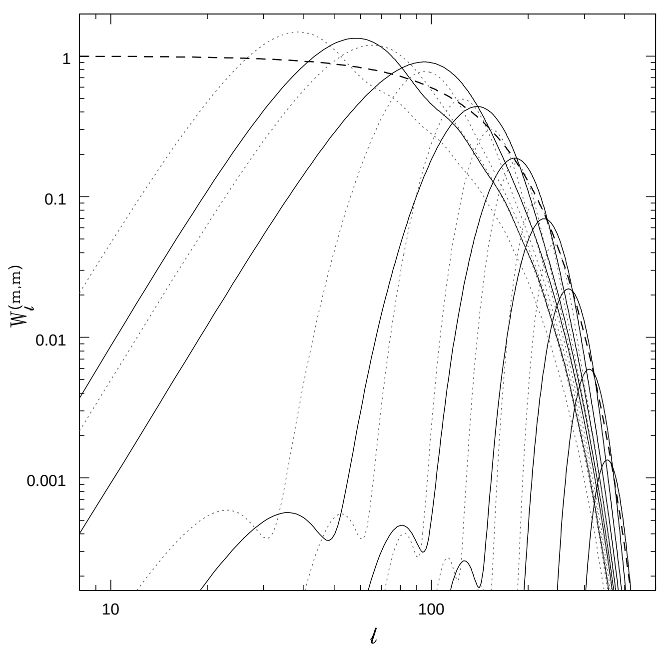

FIG. 4.—Two sets of the eight equal-modulation, exact, Python V zero-lag complete window functions $W_l^{(m,m)}(\gamma, \gamma)$. The dark solid and light dotted curves correspond to window functions at the two extreme declinations, $\delta = -63°$ and $-45°.4$, respectively. Higher modulation window functions peak at progressively larger values of l and with smaller amplitude. The dashed curve is the exact Python V zero-lag elementary window function at $\delta = -63°$. Note that higher modulation complete window functions peak at l a few times larger than the inverse beamwidth ($\sigma_{\rm rms}^{-1} \approx 140$), where the noncircularity corrections start to become important (see Fig. 2). For the same difference in azimuth the angular separation between two equal declination points ($\Delta\phi \cos\delta$) is smaller at higher $|\delta|$. Consequently, for the same modulation, the window function at $\delta = -63°$ peaks at a larger multipole than the window function at $\delta = -45°.4$.

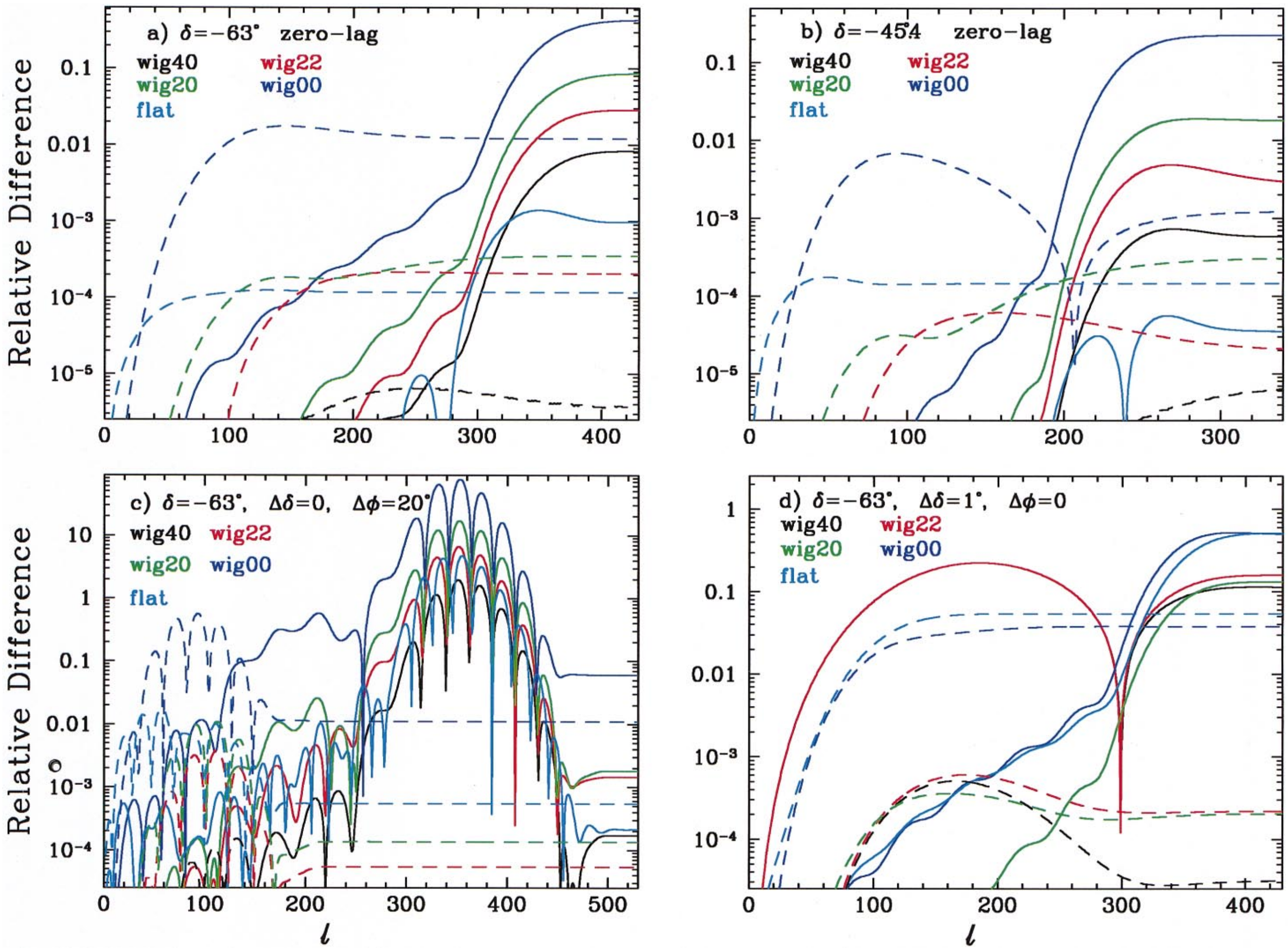

FIG. 5.—Comparisons between Python V flat bandpower equal-modulation covariance matrix elements computed using different approximations. Plotted are the relative differences between values of $F_l^{(m,\,m)}(\gamma_i, \gamma_j)$ (eq. [41]) computed using an approximate window function and those using the exact window function, normalized by dividing by the flat bandpower $C_{ij}^{(m,\,m)}$. The approximations considered are the circular-beam approximation, (wig00 in blue), the three successive leading improvements to this in the Wigner-method perturbation expansion (wig20 in green, wig22 in red, and wig40 in black; see eq. [33]. Here each successive improvement includes all lower order terms.), and the flat-sky approximation ("flat" in cyan). Two curves are shown for each approximation, corresponding to modulations 2 (*dashed curves*) and 8 (*solid curves*). At large l the modulation 8 curves converge to a lower accuracy than do the corresponding modulation 2 curves, because the noncircularity correction is more significant for higher modulations. Upper panels show differences for zero-lag covariance matrix elements at the two extreme declinations, $\delta = -63°$ (*a*) and $-45°.4$ (*b*). Lower panels show differences for nonzero-lag covariance matrix elements. Panel (*c*) corresponds to pixels separated in azimuth by 20° at declination $\delta = -63°$, and panel (*d*) corresponds to two neighboring, equal-azimuth pixels at declinations $\delta = -63°$ and $-62°$ (in panel [*d*] the solid red curve covers the solid black curve for $l \lesssim 300$). The flat-sky approximation fares well in all cases except for that of pixels separated in declination, where it fails even for small-separation pixel pairs; see panel (*d*). Panel (*d*) also shows the enormous improvement over the circular beam function approximation (wig00) achieved by accounting for even just the first-order Wigner-method correction (wig20). Panel (*c*) highlights the need to compute to a large enough value of l to achieve sufficient accuracy, i.e., truncating the circular beam function approximation (wig00) at intermediate l leads to an inaccurate result.

because these have peak sensitivity at multipoles well beyond the inverse beamwidth, which is where the noncircularity corrections start to become important (see Fig. 2).

While it is of interest to estimate the accuracy of window functions computed in various approximations, the accuracy of computed covariance matrix elements is of much greater relevance, since these directly determine the accuracy of cosmological results extracted from CMB anisotropy data. This significantly extends the range of usefulness of approximate window functions. First, the sum over l in the definition of the theoretical model covariance matrix, equation (7), averages over and hence reduces the significance of deviations between the approximate and exact window functions. For example, an approximate window function that has large deviations from the exact window function only in regimes where they oscillate in l may still result in an accurate covariance matrix. Second, errors in the window function are unimportant when the corresponding covariance matrix elements are small (subdominant). For example, while the flat-sky approximation window function is very inaccurate for a widely separated pixel pair, the covariance matrix element for such a pixel pair is subdominant and thus cannot significantly influence the results from a maximum likelihood analysis of the data. Another important consideration is the level of noise in the experiment. Because the inverse of the sum of the theoretical model and noise covariance matrices, $(C_T + C_N)^{-1}$, determines the results of the maximum likelihood analysis, the model covariance matrix must be computed to higher accuracy for an experiment with lower noise.

Equation (7) defines the model covariance matrix element $C_{ij}^{(m,n)}$ in terms of the window function and the model CMB anisotropy power spectrum. To compare covariance matrices computed using different approximations therefore requires the choice of a model C_l. We use the flat bandpower spectrum, $C_l \propto 1/l(l+1)$, for this purpose in what follows. With this choice of power spectrum, the quantity

$$F_l^{(n,m)}(\gamma_i, \gamma_j) = \sum_{l'=2}^{l} [(2l'+1)/l'(l'+1)] W_{l'}^{(n,m)}(\gamma_i, \gamma_j) \tag{41}$$

is a measure of the cumulative buildup of the corresponding covariance matrix element as one progresses with the sum over multipole l in equation (7). Up to a multiplicative normalization constant, $F_l^{(n,m)}(\gamma_i, \gamma_j)$ converges to the covariance matrix $C_{ij}^{(n,m)}$ as $l \to \infty$. Unlike W_l, F_l measures l-space information that may be directly used to estimate the accuracy of the computed covariance matrix. It also allows one to determine the value of l to which one must compute to achieve a desired accuracy.

Figure 5 compares Python V flat bandpower covariance matrix elements computed using the different approximations developed above. The upper panels, Figs. 5*a* and 5*b*, show comparisons between zero-lag covariance matrix elements.[11] At zero lag the flat-sky approximation is more accurate than the zeroth-order (circular-beam) and first-order (wig20) Wigner-method perturbation expansion approximations. The Wigner method becomes progressively more efficient (i.e., one needs to retain fewer terms in the perturbation expansion series to achieve the desired accuracy) for nonzero-lag covariance matrix elements between increasingly separated pixels. For covariance matrix elements between very widely separated pixels, even the circular-beam (zeroth-order) approximation suffices. The Wigner method is more accurate for lower modulations, which probe lower values of l where beam noncircularity corrections are smaller (see Fig. 5). The flat-sky approximation is accurate at small separations (e.g., at zero lag). For Python V, the flat-sky approximation is more accurate for pixels separated in azimuth than for pixels separated in declination. The flat-sky approximation works better for higher modulations, which probe larger values of l. The F_l curves for the circular-beam approximation (wig00) in Fig. 5*c* also highlight the possible pitfall of not computing to large enough l. Here F_{lij} does not converge to C_{ij} until $l \gtrsim 500 \sim 4\sigma_{\rm rms}^{-1}$.

7. CONCLUSION

We develop computationally rapid methods to compute the window function for a long-scan, arbitrary-beam-shape CMB anisotropy experiment. We use these methods to compute the window function for the elliptical Gaussian beam Python V experiment.

It proves convenient to separate effects due to the modulation scheme adopted from those due to the shape of the beam function by expressing the complete window function as a weighted sum of single-beam elementary window functions (eq. [10]).

Using equation (11) to obtain the exact elementary window function for a noncircular-beam experiment requires accurate computation of the spherical harmonic transform of the beam function at each pointing direction. For an experiment with a large number of pointing directions this is computationally prohibitive. For instance, Python V has 690 pixels and the scan around each is resampled at 567 points, which results in ≈ 0.4 million pointing directions. Fortunately, the 690 pixels lie on only 11 distinct elevations and the scans are performed at constant elevation. Hence, precomputing and storing the spherical harmonic beam function transforms at these 11 declinations allows for rapid computation of the exact Python V window function.

In the absence of such a simplification due to a symmetry, the Wigner-method perturbation expansion scheme allows an accurate computation of the window function with computational effort within a factor of a few of the corresponding computation for the case of a circular beam function. This factor depends on the order to which the perturbative expansion (about the circular-beam approximation) must be developed to achieve the desired accuracy. In this implementation, the Wigner method requires precomputation and storage of one spherical harmonic transform of the beam pointing at a pole, $b_{lm}(\gamma_{\rm P})$. If the beam is mildly noncircular, then for all l, $|b_{lm}(\gamma_{\rm P})|/|b_{l0}(\gamma_{\rm P})|$ falls off rapidly with increasing $|m|$, allowing for a fast and accurate transform and simpler storage. In the Appendix we record a semianalytic expression for the beam function transform for a compact elliptical Gaussian beam. In mildly noncircular cases, such as Python V, $|b_{lm}(\gamma_{\rm P})|/|b_{l0}(\gamma_{\rm P})| \to 0$ rapidly with increasing $|m|$, and the first-order Wigner method is sufficiently accurate. We also develop a flat-sky approximation for window function computation and illustrate this method by computing the Python V window function.[12] We find that the flat-sky approximation works well at zero lag and for pixels at small constant-elevation separation. At larger separations the Wigner method is more accurate than the flat-sky approximation.

The methods developed in this paper are easily extended to other cases not explicitly considered here (such as a noncircular, non-Gaussian beam and a beam that rotates on the sky, among others). Elsewhere we will summarize an analysis of the Python V data that makes use of these methods.

We acknowledge very valuable discussions with K. Coble, advice from S. Dodelson, M. Dragovan, K. Ganga, L. Knox, and the rest of the Python collaboration, comments from J.-H. P. Wu, and support from NSF Career grant AST 98-75031.

[11] Modulated zero-lag complete window functions receive contributions from nonzero-lag elementary window functions between pixels separated by as much as the chopper throw $\Phi_c = 17^\circ\!.06$.

[12] Our flat-sky approximation differs from that implemented in Coble et al. (1999) and Coble (1999).

APPENDIX A

ELLIPTICAL GAUSSIAN BEAM FUNCTION: NORMALIZATION AND TRANSFORMS

Python V is an example of an experiment with a compact, elliptical Gaussian beam function (Coble et al. 1999). In such a case it is possible to obtain accurate and useful semianalytic expressions for the Fourier transform $B(\mathbf{k})$ and the spherical harmonic transform $b_{lm}(\gamma_{\rm P})$ of the beam function.

An elliptical Gaussian beam function that is compact enough can be expressed in a locally flat-sky coordinate system (around the beam pointing direction) as

$$B(\boldsymbol{x}) = \frac{1}{2\pi\sigma_1\sigma_2}\exp\left[-\frac{x_1{}^2}{2\sigma_1{}^2} - \frac{x_2{}^2}{2\sigma_2{}^2}\right]. \tag{A1}$$

Here $\boldsymbol{x} = (x_1, x_2)$ are locally flat-sky Cartesian coordinates and σ_1 and σ_2 are the beamwidths in the $\boldsymbol{x}_1$- and $\boldsymbol{x}_2$-directions.[13] It is straightforward to establish that this is normalized so that

$$\int_{-\infty}^{\infty} dx_1 \int_{-\infty}^{\infty} dx_2 \; B(\boldsymbol{x}) = 1\ . \tag{A2}$$

We shall have need for the expression for the beam in local spherical polar coordinates $\gamma = (\theta, \phi)$, around the pointing direction which, without loss of generality, can be assumed to be the north pole $\gamma_{\rm P}$. To fix the orientation of the beam on the sky, we choose x_1 to lie along $\phi = 0$. Using the local mapping, $x_1 = \theta\cos\phi$, and $x_2 = \theta\sin\phi$, we can write

$$B(\gamma_{\rm P}, \gamma) = \frac{1}{2\pi\sigma_1\sigma_2}\exp\left[-\frac{\theta^2}{2\sigma^2(\phi)}\right], \tag{A3}$$

where the "beamwidth" is a function of the polar angle

$$\sigma^2(\phi) = [\sigma_1{}^2/(1 + \epsilon\sin^2\phi)]\ , \tag{A4}$$

and a noncircularity parameter

$$\epsilon = (\sigma_1{}^2 - \sigma_2{}^2)/\sigma_2{}^2\ . \tag{A5}$$

With the usual accurate approximation, allowed by the rapid falloff of the Gaussian in θ in equation (A3), it is straightforward to establish that the normalization condition

$$\int_0^{2\pi} d\phi \int_0^{\pi} d\theta \;\; \sin\theta \; B(\gamma_{\rm P}, \gamma) = 1 \tag{A6}$$

is satisfied for $\sigma(\phi) \ll 1$.

In the flat-sky approximation, the elementary window function defined in equation (19) depends on the Fourier transform of the beam function $B(\boldsymbol{k})$. For the elliptical Gaussian beam function of equation (A1) we find

$$B(\boldsymbol{k}) = \exp\left(-\frac{k_1{}^2\sigma_1{}^2}{2} - \frac{k_2{}^2\sigma_2{}^2}{2}\right). \tag{A7}$$

One great advantage of the flat-sky approximation is that fast Fourier transform techniques may be used to rapidly compute $B(\boldsymbol{k})$ for any beam function.

To use equation (31) to compute the curved-sky window function, we need to compute the spherical harmonic transform $b_{lm}(\gamma_{\rm P})$ of the beam function pointed at the north pole $\gamma_{\rm P}$. An elliptical Gaussian beam function results in a semianalytic expression that requires numerical evaluation of only a single integral. A more complex beam function could require a complete numerical analysis.

We first note that it is straightforward to show that

$$[b_{lm}(\gamma)]^* = (-1)^m b_{l,\,-m}(\gamma)\ . \tag{A8}$$

From equations (A3) and (12) we find

$$b_{lm}(\gamma_{\rm P}) = \frac{(-1)^{-m}}{2\pi\sigma_1\sigma_2}\left[\frac{2l+1}{4\pi}\frac{(l+m)!}{(l-m)!}\right]^{1/2}\int_0^{2\pi} d\phi\; e^{-im\phi}\int_0^{\pi} d\theta \;\; \sin\theta\; e^{-\theta^2/[2\sigma^2(\phi)]}P_l^{-m}(\cos\theta)\ , \tag{A9}$$

where we have used the usual expression for Y^*_{lm} in terms of the associated Legendre function P_l^{-m}. For a compact beam and for large l, the θ integral may be performed using the usual small-θ approximation,

$$\lim_{l\to\infty} l^m P_l^{-m}(\cos\theta) = J_m([l + 0.5]\theta)\ , \tag{A10}$$

[13] The beam function is also a function of the pointing direction $\mathbf{x}_0$, $B(\mathbf{x}_0, \mathbf{x})$, taken to be at the origin here.

e.g., equation (8.722.2) of Gradshteyn & Ryzhik (1994). Using equation (6.631.7) of Gradshteyn & Ryzhik (1994), we find

$$b_{lm}(\gamma_{\rm P}) = \frac{(-l)^{-m}}{\pi(l+0.5)^{3/2}}\left[\frac{(l+m)!}{(l-m)!}\right]^{1/2}\frac{1}{\sigma_1\,\sigma_2}\int_0^{2\pi} d\phi\ e^{-im\phi}f^3(\phi)\exp -f^2(\phi)[I_{(m-1)/2}(f^2(\phi)) - I_{(m+1)/2}(f^2(\phi))]\ , \tag{A11}$$

where I_ν is the modified Bessel function and

$$f(\phi) = [(l+0.5)\sigma(\phi)]/2\ . \tag{A12}$$

Equation (A11) is valid for $m \geq 0$; for $m < 0$ we use this and equation (A8) for the b_{lm}-values. It is straightforward to show that for a circular-beam equation (A11) reduces to the well-known expression.

Using the reality condition on the beam, equation (A8), one may show that the $\int_0^{2\pi} d\phi$ integral in equation (A11) may be replaced by a $[1+(-1)^{-m}]\int_0^{\pi} d\phi$ integral. Clearly, the $b_{lm}(\boldsymbol{x}_3')$-values vanish for odd m.[14] Since $f(\phi)$ is a function of $\sin^2(\phi)$, it is straightforward though tedious to show that the imaginary part of $e^{-im\phi}$ in equation (A11) leads to an expression that vanishes. Thus we have

$$b_{lm}(\gamma_{\rm P}) = \frac{[1+(-1)^{-m}](l)^{-m}}{\pi(l+0.5)^{3/2}}\left[\frac{(l+m)!}{(l-m)!}\right]^{1/2}\frac{1}{\sigma_1\,\sigma_2}\int_0^{\pi} d\phi\ \ \cos(m\phi)f^3(\phi)\exp -f^2(\phi)[I_{(m-1)/2}(f^2(\phi)) - I_{(m+1)/2}(f^2(\phi))]\ . \tag{A13}$$

For an elliptical Gaussian beam function, this approximate semianalytic spherical harmonic transform agrees well with the exact, fully numerical transform.

[14] This is true provided the integral does not diverge. In fact, it is straightforward to establish that it is integrable. We use $e^{im\phi} = \cos(m\phi) + i\sin(m\phi)$ and consider the real and imaginary parts separately. Both of these are continuous functions of ϕ over $0 < \phi < \pi$ and are thus Riemann integrable over this interval (see pp. 42 and 63 of Whittaker & Watson 1969).

REFERENCES

Aghanim, N., Forni, O., & Bouchet, F. R. 2001, A&A, 365, 341
Bond, J. R., & Efstathiou, G. 1987, MNRAS, 226, 655
Bond, J. R., Jaffe, A. H., & Knox, L. 2000, ApJ, 533, 19
Coble, K. 1999, Ph.D. thesis, Univ. Chicago
Coble, K., et al. 1999, ApJ, 519, L5
Dawson, K. S., Holzapfel, W. L., Carlstrom, J. E., Joy, M., LaRoque, S. J., & Reese, E. D. 2001, ApJ, 553, L1
Dodelson, S. 2000, Int. J. Mod. Phys. A, 15, 2629
Douspis, M., Bartlett, J. G., Blanchard, A., & Le Dour, M. 2001, A&A, 368, 1
Fischler, W., Ratra, B., & Susskind, L. 1985, Nucl. Phys. B, 259, 730
Ganga, K., Ratra, B., Gundersen, J. O., & Sugiyama, N. 1997, ApJ, 484, 7
Ganga, K., Ratra, B., Lim, M. A., Sugiyama, N., & Tanaka, S. T. 1998, ApJS, 114, 165
Ganga, K., Ratra, B., & Sugiyama, N. 1996, ApJ, 461, L61
Gawiser, E., & Silk, J. 2000, Phys. Rep., 333, 245
Górski, K. M., Ratra, B., Stompor, R., Sugiyama, N., & Banday, A. J. 1998, ApJS, 114, 1
Górski, K. M., Ratra, B., Sugiyama, N., & Banday, A. J. 1995, ApJ, 444, L65
Gradshteyn, I. S., & Ryzhik, I. M. 1994, Table of Integrals, Series, and Products, ed. A. Jeffrey (5th ed.; San Diego: Academic Press)
Knox, L. 1999, Phys. Rev. D 60, 103516
Knox, L., & Page, L. 2000, Phys. Rev. Lett., 85, 1366
Lineweaver, C. H. 2001, in ASP Conf. Ser. 237, Gravitational Lensing: Recent Progress and Future Goals, ed. T. G. Brainerd & C. S. Kochanek (San Francisco: ASP), in press
Mukherjee, P., Hobson, M. P., & Lasenby, A. N. 2000, MNRAS, 318, 1157
Padin, S., et al. 2001, ApJ, 549, L1
Park, C.-G., Park, C., Ratra, B., & Tegmark, M. 2001, ApJ, 556, 582
Phillips, N. G., & Kogut, A. 2001, ApJ, 548, 540
Podariu, S., Souradeep, T., Gott, J. R., III, Ratra, B., & Vogeley, M. S. 2001, astro-ph/0102264
Ratra, B., Ganga, K., Sugiyama, N., Tucker, G. S., Griffin, G. S., Nguyên, H. T., & Peterson, J. B. 1998, ApJ, 505, 8
Ratra, B., Stompor, R., Ganga, K., Rocha, G., Sugiyama, N., & Górski, K. M. 1999, ApJ, 517, 549
Ratra, B., Sugiyama, N., Banday, A. J., & Górski, K. M. 1997, ApJ, 481, 22
Rocha, G. 1999, in Dark Matter in Astrophysics and Particle Physics 1998, ed. H. V. Klapdor-Kleingrothaus & L. Baudis (Bristol: Inst. Phys. Publ.), 238
Rocha, G., Stompor, R., Ganga, K., Ratra, B., Platt, S. R., Sugiyama, N., & Górski, K. M. 1999, ApJ, 525, 1
Romeo, G., Ali, S., Femenía, B., Limon, M., Piccirillo, L., Rebolo, R., & Schaefer, R. 2001, ApJ, 548, L1
Subrahmanyan, R., Kesteven, M. J., Ekers, R. D., Sinclair, M., & Silk, J. 2000, MNRAS, 315, 808
Tegmark, M., & Zaldarriaga, M. 2000, ApJ, 544, 30
Varshalovich, D. A., Moskalev, A. N., & Khersonskii, V. K. 1988, Quantum Theory of Angular Momentum (Singapore: World Scientific) (VMK)
Whittaker, E. T., & Watson, G. N. 1969, A Course of Modern Analysis (New York: Cambridge Univ. Press)
Wu, J.-H. P., et al. 2001a, ApJS, 132, 1
———. 2001b, astro-ph/0104248

Note added in proof.—It is possible to obtain an analytical expression for the spherical harmonic transform $b_{lm}(\gamma_{\rm P})$ of the elliptical Gaussian beam, equation (A1), pointed at the north pole $\gamma_{\rm P}$. This is

$$b_{lm}(\gamma_{\rm P}) = \left[\frac{2l+1}{4\pi}\frac{(l+m)!}{(l-m)!}\right]^{1/2}(l+1/2)^{-m}I_{m/2}\left[\frac{(l+1/2)^2\sigma_1^2\epsilon}{4(1+\epsilon)}\exp\left\{-\frac{(l+1/2)^2\sigma_1^2}{2}\left[1-\frac{\epsilon}{2(1+\epsilon)}\right]\right\}\right.\ , \tag{A14}$$

Here ϵ is the noncircularity parameter of equation (A5) and I_ν is the modified Bessel function. The above results, derived using the same set of assumptions as the semianalytic result of equation (A11), is numerically identical to it. It corresponds to using the flat-sky Fourier transform of a compact beam and relating Fourier coefficients to spherical multipoles. We thank A. Challinor for bringing this result to our attention.